ROYAL SOCIETY OF CHEMISTRY

PAPER

Check for updates

Membrane deformation and layer-by-layer peeling of giant vesicles induced by the pore-forming toxin pneumolysin†

Patrick Drücker, [ID] *[a,b] Ioan Iacovache,[c] Simon Bachler,[a] Benoît Zuber, [ID] [c] Eduard B. Babiychuk,[b] Petra S. Dittrich [ID] [a] and Annette Draeger[b]

Protein–membrane interactions that modify the shape of membranes are important for generating curvature, membrane deformation by protein–protein crowding or trafficking of vesicles. Giant vesicles represent a simplified but versatile model for biological membranes and are commonly employed for the study of lipid domains and permeation across compartments. In this study, we investigated the interaction of pneumolysin (PLY), a pore-forming toxin secreted by S*treptococcus pneumoniae*, with multilamellar and unilamellar membranes. It reveals an enlargement of membrane area due to the insertion of pores into the bilayer and protein–membrane aggregations that induce membrane deformation and wrinkling. Moreover, we demonstrate that PLY peel-off layers from multilamellar giant vesicles in a hitherto unknown layer-by-layer peeling mechanism, which reveals the structure and number of membrane lamellae. We employed microfluidic methods to capture giant vesicles and confocal laser scanning microscopy, transmission microscopy, dynamic light scattering and cryo-electron microscopy to disclose the structure of multilamellar vesicles. Based on our findings we suggest how back-to-back pore arrangements stabilize large PLY–membrane entities and that pore-displaced lipids possibly remain in the membrane.

Introduction

The interactions of pore-forming toxins (PFTs) with biological membranes, that include membrane binding, the re-organization during pore formation and barrier disintegration were often investigated to analyze the mechanism of membrane perforation and the pathogenicity on cells.[1–4] The pore-forming toxin, pneumolysin (PLY), secreted by S*treptococcus pneumoniae*, can cause severe pneumonia or meningitis in humans.[5] As a member of the cholesterol-dependent cytolysins (CDCs), PLY is secreted as a soluble monomer, which binds to cholesterol in cellular membranes, self-assembles to oligomers and forms pre-pores which eventually transform to large active pores.[5,6] These pores finally promote cell lysis and death.[7]

In addition to pore formation, previous studies also revealed remarkable protein-induced structural modifications of biological membranes, such as membrane bending by protein–protein crowding,[8,9] the rolling of supported membranes as a result of

annexin proteins causing membrane curvature[10] or cytochrome c collapsing specific domains on giant vesicles.[11] Interestingly, also membrane-active, antimicrobial peptides could promote strain-induced membrane lysis after pore formation.[12] In general, PLY is well known for the perforation of membranes by the formation of holes, but membrane deformation or peeling of multilamellar membranes has not been observed nor addressed in detail.[6,13–16]

Furthermore, PLY has been regularly employed to investigate cellular repair mechanisms,[17,18] including calcium-dependent plasma membrane repair,[19] active microvesicle shedding[20] or the blebbing of cellular membranes.[21] Recently, we demonstrated that cell repair mechanisms advance from an inhomogeneous binding of non-lytic PLY concentrations to plasmalemmal, cholesterol-rich domains.[22]

In order to address PFT–membrane interactions, giant unilamellar vesicles (GUV) are used as a model to represent biological bilayer membranes and cellular curvature.[23,24] Although, the term GUV is regularly used, exact unilamellarity is not always assured. For instance, vesicles generated by swelling methods may have a variable number of lamellae.[25] However, the lamellarity of membranes is important when vesicle permeation by PFTs or other permeation studies are investigated.

Many protein–membrane interactions, including permeation analysis, were recently addressed by employing the advantages of microfluidic devices.[26–28] These comprise the ability to control incubation into sorted compartments while

*a*Department of Biosystems Science and Engineering, ETH Zurich, 4058 Basel, Switzerland. E-mail: patrick.druecker@bsse.ethz.ch
*b*Department of Cell Biology, Institute of Anatomy, University of Bern, Baltzerstrasse 2, 3000 Bern 9, Switzerland
*c*Laboratory of Experimental Morphology, Institute of Anatomy, University of Bern, Baltzerstrasse 2, 3000 Bern 9, Switzerland

immobilizing vesicles without chemical tethers. In addition microfluidic devices are well compatible with high-resolution fluorescence imaging techniques.[29–31]

Herein, we investigated protein–membrane interactions of pneumolysin on individual multilamellar giant vesicles in a microfluidic device and show protein–membrane aggregation that induces membrane wrinkling and membrane surface enlargements. These effects led to an unexpected layer-by-layer peeling, which reveals the number of lamellae of giant vesicles. Furthermore, we discriminate between different multilamellar membranes and predict the number of lamellae by employing transmission wide field microscopy without being restricted by occasional photo bleaching during prolonged observation.[32]

Results

Phosphatidylcholines are the most prevalent lipids in eukaryotic cell plasma membranes[33,34] and are widely used for membrane model systems such as giant vesicles.[35–39] Thus, we con-

firmed binding of pneumolysin to large unilamellar vesicles containing either unsaturated di-oleoyl-phosphatidylcholine (DOPC) or saturated di-palmitoyl-phosphatidylcholine (DPPC) and cholesterol for the membrane models applied herein (Fig. 1). Binding of PLY on vesicles is demonstrated by the inhibition of hemolysis, where liposomes are pre-incubated with pneumolysin and then exposed to human red blood cells. This competition binding assay measures the release of hemoglobin from lysed erythrocytes.[22,40] The membrane affinity thus depends on the accessibility of the receptor cholesterol for PLY binding and is affected by cholesterol concentration and the lipid acyl-chain saturation (Fig. 1; Table SI 1†) as also shown on different, sphingomyelin containing liposomes.[22] A plausible current explanation how this accessibility might be determined by cholesterol concentration and lipid saturation, is illustrated in Fig. 1A. It takes into account that cholesterol has less area per molecule in membranes at high concentrations[41,42] meaning that shielding of cholesterol by bulky lipid head groups towards water exposure is less effective in an unsaturated lipid environment and at high cholesterol
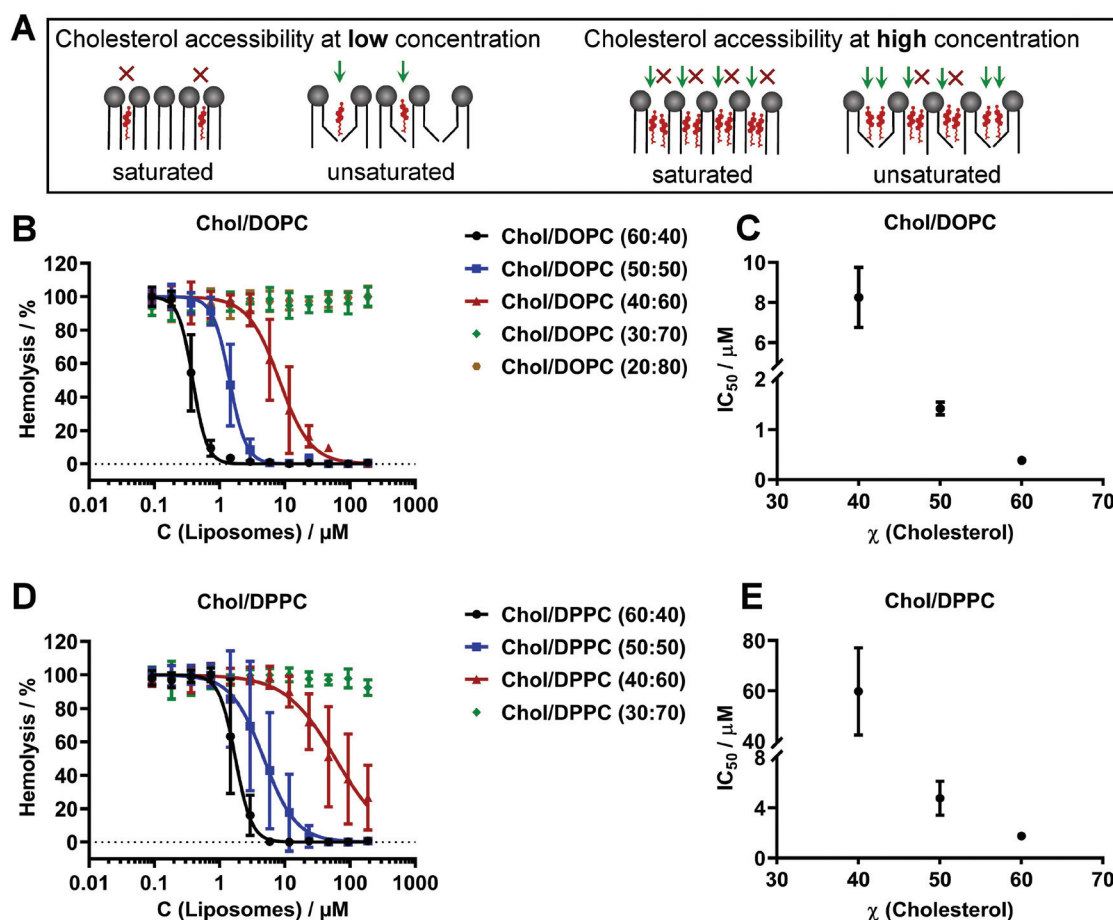
Fig. 1 Cholesterol-dependent binding of pneumolysin to phosphatidylcholine-containing liposomes. A: Sketch illustrating the relative accessibility of cholesterol for PLY binding in dependence of lipid saturation and cholesterol concentration. B, D: The hemolytic activity after pre-incubation of PLY with DOPC or DPPC containing large unilamellar liposomes. C, E: The half-maximal inhibitory concentrations required to prevent hemolysis (IC_{50}) of DOPC or DPPC and cholesterol containing LUVs depend on the amount of cholesterol. Each curve represents the results of 3 to 5 independent experiments, each performed in triplicate and IC_{50} determination is the result of nonlinear regression of dose–response curve fittings to the data in B, D. Error bars represent standard deviation (SD).

concentration, which in turn affects PLY binding. This is demonstrated by the comparison of effective half-maximal inhibitory coefficients (IC_{50}) measured by liposome pre-sequestration (Fig. 1B–D). For instance, the IC_{50} value (1.4 ± 0.1 μM) for PLY binding to a less ordered DOPC/Chol (50 : 50) membrane is smaller than $IC_{50} = 4.8 \pm 1.4$ μM for a more ordered DPPC/Chol (50 : 50) membrane and hence indicates a higher affinity (accessibility) (Fig. 1C and E; Table SI 1†).

Protein–membrane aggregation and layer-by-layer peeling of giant vesicles

Association of mCherry–PLY with unilamellar giant vesicles of a homogeneous, binary lipid mixture previously showed a homogeneous distribution during initial binding and formation of active pores.[22] Likewise, binding of 320 nM mCherry–PLY to multilamellar giant vesicles (DOPC/Chol, 50 : 50) appears to be initially homogeneous. Prolonged incubation of vesicles trapped in a microfluidic device (Fig. SI 1†) with mCherry-PLY for more than 30 seconds induced the formation of protein–membrane aggregates (Fig. 2A and B). This eventually led to PLY-induced membrane deformation and wrinkling (Fig. 2B, blue arrow) until rupture of the outer layer occurs during continued incubation (Fig. 2B, yellow arrows). Furthermore, large PLY–membrane aggregates and tubule-like structures were attached to the vesicle surface (Fig. 2B, green arrows), which expanded during continued incubation (Fig. 2B).

PLY-induced ripping of the outer membrane was accompanied by layer-by-layer peeling (Fig. 2C, arrows; Video SI 1†). While the outer, peeling layer wrinkled (Fig. 2B and C, blue arrows), the newly exposed layer presented initial homogeneous PLY binding (Fig. 2C, 00:50–01:10 min) until the cycle of membrane deformation, wrinkling and layer-peeling repeats (Video SI 1†). The rupture of layers is induced when protein–protein and protein–membrane interactions between pores induced strain on the bilayer that exceeds the energy barrier of membrane stability. This is the case when membrane wrinkles were formed by protein–membrane aggregation (Fig. 2C, blue arrows) and the relative amount of pneumolysin on the surface reaches a threshold of at least 50–60% fluorescence intensity (Fig. 2D).

The comparison of maximum-intensities in cross-sectional line profiles, which were deduced from transmission bright field microscopy, demonstrated that the number of membrane lamellae shrinks when peeling occurs (Fig. 2E). This is similar to methods based on contrast imaging and changes in refractive index[43] but is independent from the analysis of fluorescence intensity.[25] For instance, the membrane lamellarity, *i.e.* the intensity in transmission microscopy was reduced after 06:29 min PLY incubation time compared to 00:45 min incubation time on the same vesicle (Fig. 2E, grayscale images, line sections and line profiles). Here, several layer-by-layer peeling events took place in between (Video SI 1†).

In comparison to vesicles of unsaturated DOPC and cholesterol (50 : 50) (Fig. 2), a similar lipid composition containing the same amount of cholesterol but saturated DPPC, showed less intensive mCherry–PLY binding and no membrane wrinkling nor peeling of the outer layer even during prolonged incu-

bation time under similar conditions (Fig. SI 2†). The PLY affinity of DPPC/Chol (50 : 50) liposomes, $IC_{50} = 4.8 \pm 1.4$ μM is approximately 3.4-fold lower than the affinity towards DOPC/Chol (50 : 50), $IC_{50} = 1.4 \pm 0.1$ μM liposomes (Fig. 1C and E; Table SI 1†). Thus, the capability of PLY to deform and peel off the membrane of a multilamellar giant vesicle correlates with the binding activity and membrane order (Fig. 1; Fig. SI 2†).

In order to analyze whether the formation of active pores is important for membrane aggregation and peeling, we probed several PFTs. First, to confirm that the observed membrane interactions are not an inherent property of mCherry-tagged PLY, we tested wild-type PLY that showed similar protein–membrane aggregation of Bodipy-PC labeled membranes and could induce peeling (Fig. SI 3A†). Secondly, another CDC, listeriolysin-O, also induced membrane deformation, -aggregation (Fig. SI 3B,† arrow), as well as -peeling (Video SI 2†).

In contrast, inactive PFTs showed a different behavior. The pneumolysin mutant EGFP-ΔA146R147-PLY (NT-PLY) binds cholesterol, oligomerizes but cannot transform into active pores.[44] It has a similar membrane binding affinity than wt-PLY, since it prevents hemolysis by wt-PLY when being pre-incubated on erythrocytes.[44] Binding of 340 nM NT-PLY on DOPC/Chol (50 : 50) giant vesicles for 32 min showed only minor membrane deformations (Fig. SI 3C; Video SI 3†). These were not as pronounced as aggregations induced by active, pore-forming PLY within 17 min under similar conditions (Fig. 2B; Fig. SI 3A†). In addition, we compared that result with another inactive pore-forming toxin, EGFP-NT-LYS[45,46] which binds sphingomyelin within membranes but is unable to transform into pores. Incubation of 322 nM EGFP-NT-LYS on vesicles that contained a similar amount of the receptor, oleoyl-sphingomyelin (OSM) (OSM/Chol, 50 : 50) shows coverage of the membrane surface, but was not able to induce protein–membrane aggregation, -wrinkling or -peeling (Fig. SI 3D, Video SI 4†). Together these findings suggest that the capability of pore-forming toxins such as pneumolysin, to induce large protein–membrane aggregates and membrane wrinkling is determined by the pore-forming activity and is distinct from simple membrane binding.

PLY-induced peeling reveals the number of membrane layers

The peeling itself was recognized by movement of the aggregated membrane and when a new, initially homogeneous PLY-binding membrane becomes exposed underneath (Fig. 2; Fig. 3A). Permeation, demonstrated by FITC-dextran that enters the lumen of giant vesicles occurs when the outer layer rips apart and exposes the last underlying layer for PLY association (Fig. 3A, red arrow; Fig. 3B), at 1:05–1:10 min incubation time. The number of membrane lamellae is reduced during this single peeling event, as confirmed by analysis of line profiles across the vesicle rim from transmission bright field microscopy (Fig. 3B). In this case, the permeated vesicle initially contained two layers. Additionally, the time of PLY incubation which was required to permeate giant vesicles, increased with the number of layers (Fig. 3C).

The number of layers that peeled off an individual giant multilamellar vesicle was counted, when it showed several
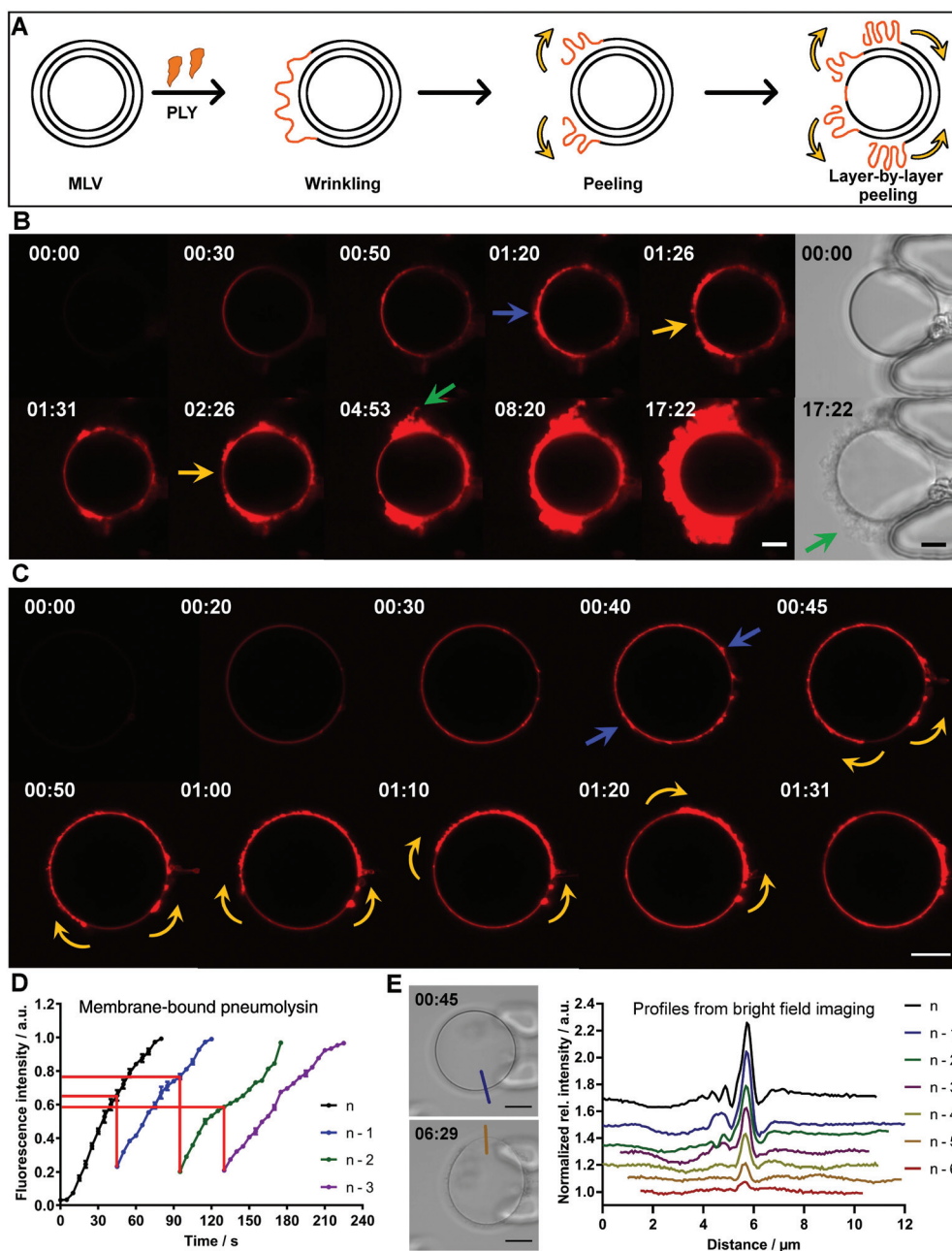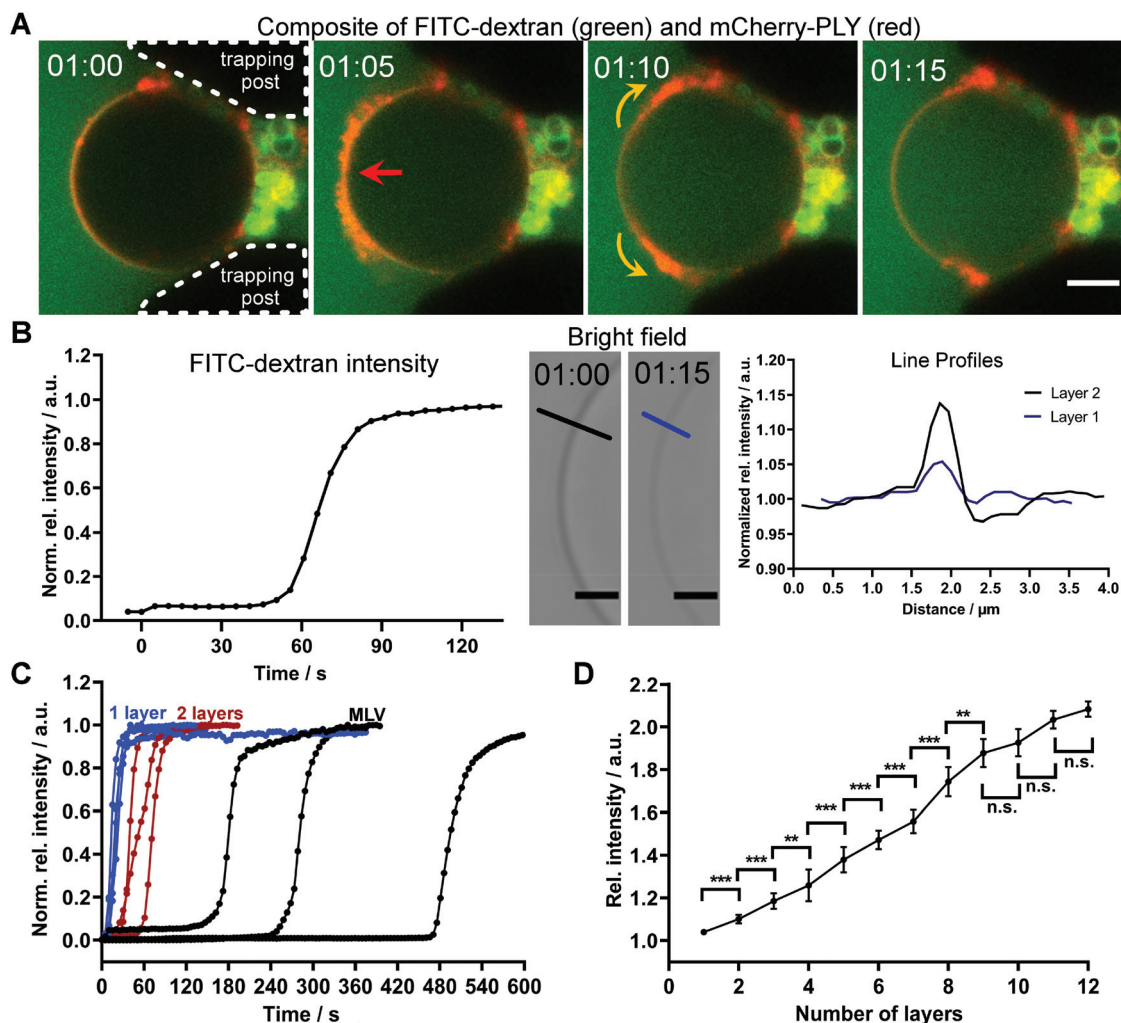
Fig. 2 PLY induced protein–membrane aggregation and layer-by-layer peeling of giant vesicles. A: Sketch illustrating PLY-induced membrane wrinkling and layer-by-layer peeling. B: A giant vesicle of DOPC/cholesterol (50 : 50) is trapped in the microfluidic device and incubated with mCherry-PLY (320 nM, red). PLY binding followed membrane wrinkling and the formation of protein–membrane aggregates (blue arrow), few layer peelings (rupture of outer layer, yellow arrows), final large surface aggregation (image at 17:22 min), which hindered further peeling and tubule structures (green arrows). Scales = 5 μm. The grayscale micrographs are bright-field transmission images. C: A giant vesicle (DOPC/cholesterol, 50 : 50) showing layer-by-layer peeling events during mCherry-PLY (320 nM, red) incubation. Yellow arrows indicate the movement of the outer membrane layer during one peeling event. The newly exposed layer shows initial homogeneous PLY binding (00:50). Scale = 10 μm. D: The relative fluorescence intensity of membrane bound mCherry-PLY during initial binding to the outer layer (black), followed by the intensity of underlying membranes (blue, green, purple) after three subsequent peeling events of the vesicle shown in C. Red lines highlight the relative intensity when a layer tears; the outer black layer ruptured at ≈65% intensity and revealed a new layer underneath (blue). E: Two bright-field transmission images of the vesicle shown in C with line profiles measured perpendicular to the membrane rim. The line profiles deduced from bright-field transmission images denote six peeling events starting from the initial multilamellar membrane (n) (stacked graph). Scales = 10 μm. Time = mm:ss. Images representative for n = 8.

sequential layer-by-layer peeling events. In these cases, the relative membrane intensities of transmission bright field microscopy were reduced in a linear manner (Fig. SI 4A†).

Moreover, the influx of FITC-dextran into the vesicle lumen marked the last layer. This happened rapidly if only one final layer was exposed to PLY. In combination with the number of

Fig. 3 The signal intensity of the vesicle membrane rim deduced from bright field transmission microscopy correlates with the number of layers. A: A two layer giant vesicle (DOPC/Chol, 50 : 50, 0.05% Bodipy-PC) shows strong protein–membrane aggregation and wrinkling in the presence of mCherry-PLY (320 nM) (red), until the outer layer rips eventually apart (here at 01:05 min, red arrow and 01:10 min, yellow arrows). The FITC dextran intensity (green) in the vesicle's lumen strongly increased during this event, while the potential, last membrane layer remains stable and binds PLY homogeneously. Scale = 5 μm. B: The relative inner FITC-dextran fluorescence intensity of the vesicle shown in A, which rises when the outer layer peels apart. The membrane rim of the bright field transmission micrographs is less intense after the layer has peeled off (equatorial confocal microscopy sections and line profiles as marked). Scale = 2 μm. C: PLY-induced FITC-dextran translocation through a giant unilamellar vesicle, which did not peel (blue), two layer vesicles (red) with one peeling event and MLVs (black). D: The relative maximum intensity of equatorial membrane line profiles deduced from giant vesicles in relation to the number of layers. $n = 49$. PLY-induced layer-by-layer peeling events of 1–7 layers of several DOPC/cholesterol (50 : 50) vesicles were analyzed. *** $P < 0.001$, ** $P < 0.01$, n.s. = not significant. Error bars are S.D. Time = mm:ss. Images representative for $n = 4$.

subsequent peeling events and knowledge of when the last layer was exposed, the total number of lamellae on the vesicle was revealed (Fig. 3A; Fig. SI 4A, GV-7†). Individual, subsequent layer-by-layer peeling events were grouped according to similar intensity (Fig. SI 4B†). Interestingly, the membrane rim maximal intensities in transmission bright field microscopy for the layers 1–9 of multilamellar giant vesicles were distinct from each other (Fig. 3D). Thus the number of lamellae of giant vesicles could be determined without being compromised by disadvantages of fluorescence measurements, such as photo bleaching.

Interconnection of membranes by back-to-back pore association

Prolonged incubation of PLY on vesicles which have multiple layers led to the formation of very large protein–membrane wrinkles and tubules (Fig. 4A and Fig. SI 3A†) that contain permeated, FITC-dextran filled cavities (Fig. 4A, arrow). These structures may grow until they exceed the size of the original vesicle (Fig. SI 3A†). This could not be observed on unilamellar giant vesicles, showing that enough membrane material is required as a source (discussed below).
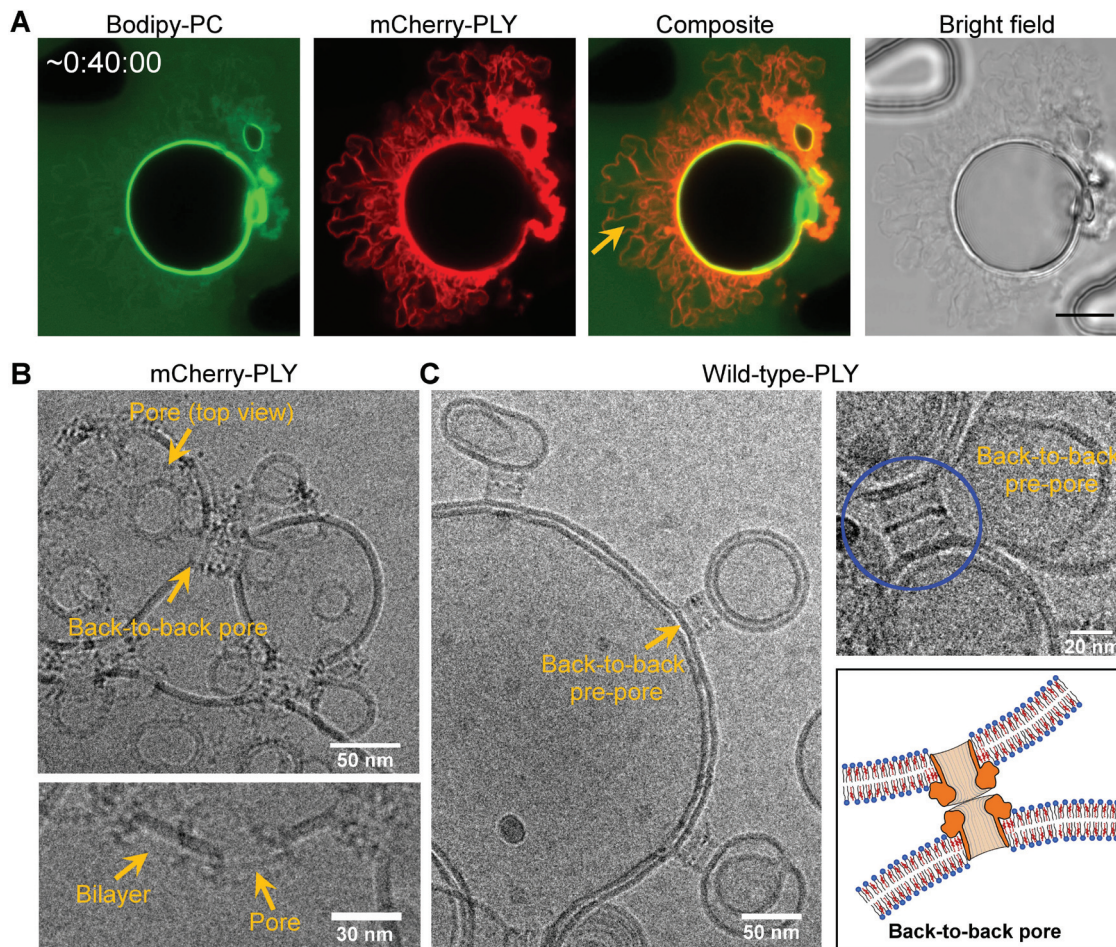
Fig. 4 Pneumolysin membrane organization and back-to-back pores interconnecting DOPC and cholesterol-containing membranes. A: Large membrane wrinkles and tubules after prolonged incubation of a giant vesicle (DOPC/cholesterol, 50 : 50 and 0.05 mol% Bodipy-PC) with mCherry-PLY (320 nM) in the presence of 0.5 mg ml^{-1} FITC-dextran. Scale = 10 μm. FITC-dextran-filled cavities are formed between membrane layers (arrow). B: Transmission electron micrographs showing back-to-back pores interconnecting two adjacent bilayers of DOPC/cholesterol (50 : 50) (2 mM in PBS), incubated with mCherry-PLY (1 μM). Side-view and top-view representations of pores. C: Transmission electron micrographs showing back-to-back pre-pores interconnecting two adjacent bilayers of DOPC/cholesterol (60 : 40) (2 mM in PBS), incubated with wild-type-PLY (1 μM). Blue circle: Back-to-back pre-pore and back-to-back pore sketch. Representative images for $n = 4$.

Previously, on microvesicles that have been shed from cellular membranes during plasmalemmal repair, a back-to-back association of wild-type PLY pores interconnecting two adjacent bilayers was observed.[20] Therefore, we analyzed pore formation and back-to-back pore arrangements of mCherry–PLY and wild-type PLY on DOPC and cholesterol-containing membranes by transmission cryo-electron microscopy (Fig. 4B and C). Both, PLY pores as well as PLY-pre-pores form back-to-back arrangements that interconnect adjacent bilayers (Fig. 4). Pores were clearly distinguished from intact bilayer fragments (Fig. 4) and led to linkage of membranes in a close vicinity of about 25 ± 1.1 nm distance, thus demonstrating that PLY itself is sufficient to interconnect lipid membranes. These protein–protein interactions seem to promote strain on protein–membrane aggregated outer layers of multilamellar vesicles as discussed above.

Layer-by-layer peeling of multilamellar giant vesicles as demonstrated herein indicates that multiple membrane bilayers

must be aligned together. This was confirmed on PLY free, large multilamellar liposomes of DOPC/Chol (50 : 50) where several layers were packed in very close vicinity (Fig. SI 5†).

Membrane enlargement by binding and perforation of pneumolysin

During the interaction of PLY pores with membranes some vesicles occasionally deform and collapse, showing that PLY disintegrated the membrane structure (Fig. SI 6A,† 01:10 min). This is possibly induced by the formation of many pores and immediate protein–membrane aggregation. Interestingly, we also observed a significant enlargement of the vesicle diameter. Incubation of 320 nM mCherry–PLY on a DOPC/Chol (50 : 50) unilamellar giant vesicle led to an increase in diameter from 17.3 ± 0.18 μm to 23.2 ± 0.18 μm within 40 seconds (Fig. 5A), followed by a structural disintegration and vesicle collapse (Fig. SI 6B, 07:20 min; Video SI 5†). The membrane enlarges simultaneously with the formation of active pores (Fig. SI 6C,
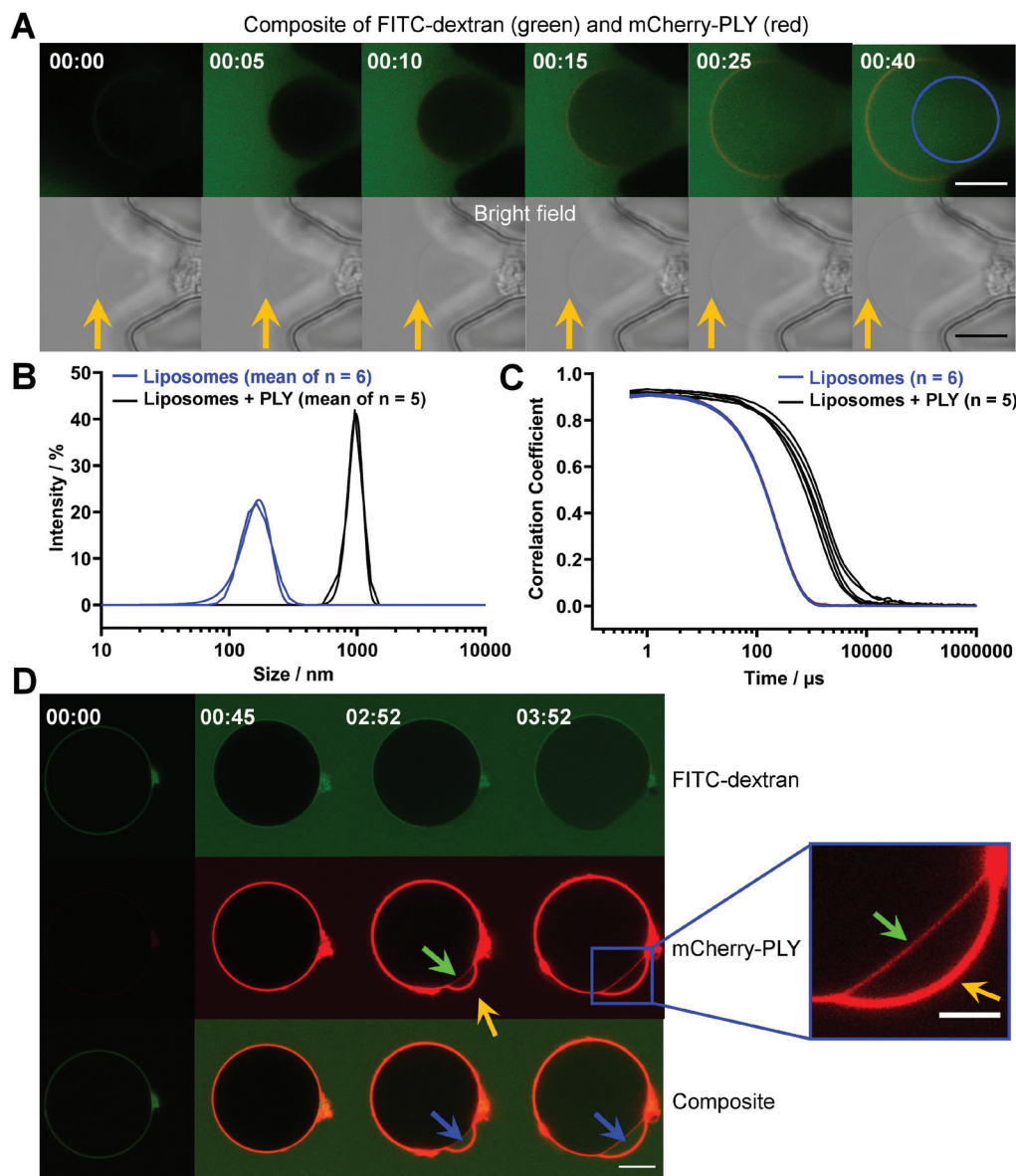
Fig. 5 Pneumolysin-induced enlargement of vesicle membranes. A: Enlargement of a unilamellar giant vesicle (DOPC/Chol, 50 : 50, 0.05% Bodipy-PC) in response to mCherry-PLY (320 nM, red) incubation in the presence of 0.5 mg ml^{-1} FITC-dextran. The blue circle refers to the original vesicle size before treatment. Scale = 10 μm. B: Mean size distribution of large unilamellar liposomes (DOPC/Chol, 50 : 50, 0.25 mM in PBS) (blue) and the same liposomes incubated with 500 nM PLY after 5 min incubation (black), measured by dynamic light scattering. A Gaussian distribution was determined as shown. C: DLS correlation data of all the individual measurements which are summarized in B. D: Formation of a large membrane bleb with an interlayer cavity on a multilamellar giant vesicle (DOPC/Chol, 60 : 40, 0.05% Bodipy-PC), in response to mCherry-PLY (320 nM, red) incubation in the presence of 0.5 mg ml^{-1} FITC-dextran. Contrast enhanced to highlight PLY on the underlying layer. Scale = 10 μm; zoom = 5 μm. Incubation times = mm:ss. Images representative for n = 3.

FITC-dextran influx, Video SI 6†). A similar effect was also demonstrated on vesicles, which showed several peeling events before the enlargement took place (Video SI 1,† at approx. 07:00 min).

In addition, we performed dynamic light scattering (DLS) experiments, that could be employed to determine the size distribution of liposomes.[47,48] The hydrodynamic radius of large unilamellar liposomes (LUVs) which had a size of Ø = 170 ± 42 nm, increased to a diameter of Ø = 975 ± 130 nm after incubation with 500 nM PLY (Fig. 5B and C). Thus, the

hydrodynamic radius of liposomes incubated with pneumolysin increased approximately 5-fold. In contrast, the hydrodynamic radius of similar liposomes which originally had a size of Ø = 185 ± 53 nm, only moderately increased to a diameter of Ø = 231 ± 61 nm after treatment with 500 nM non-pore-forming NT-PLY (Fig. SI 7†). This suggests that pneumolysin increases the size of liposomes predominantly by membrane insertion and pore formation and probably through aggregation *via* pores (Fig. 4B and C).

The enlargement of the outer layer of a multilamellar vesicle can promote the formation of a large membrane bleb that contains an aqueous cavity between layers (Fig. 5D, yellow arrows). This cavity eventually becomes filled by FITC-dextran (blue arrows) due to the formation of pores on the outer membrane. Here, PLY monomers diffused through pores on the
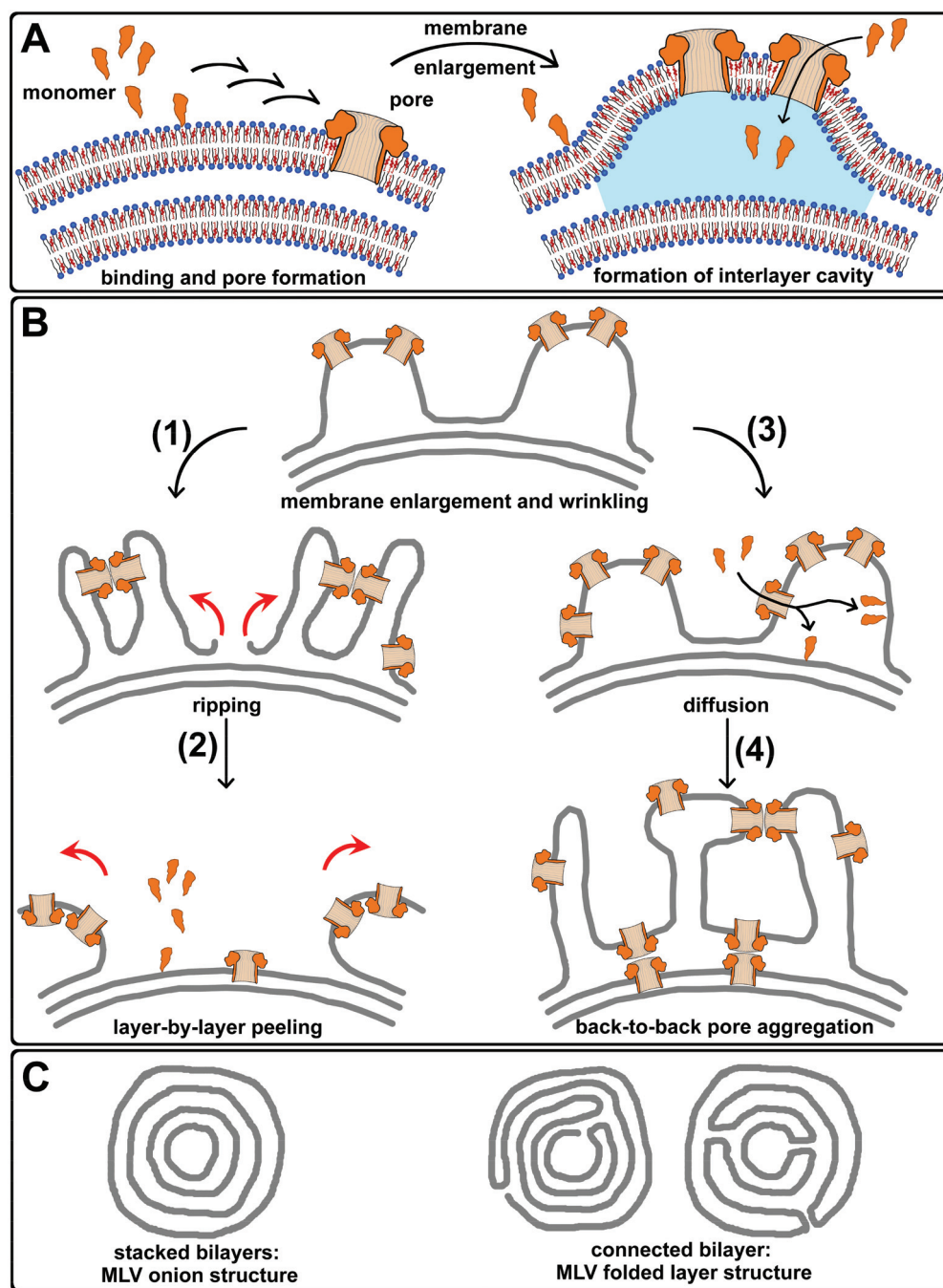
Fig. 6 Pneumolysin–membrane aggregation and peeling of giant vesicles. A: Pneumolysin (orange) binds the outer layer of a multilamellar vesicle, oligomerizes and performs the transition from pre-pores to active pores (small arrows). PLY binding and pore formation leads to an aerial expansion of the vesicles outer membrane, which results in the formation of PLY–membrane wrinkling and a cavity between membranes (blue). PLY monomers pass through existing pores, entering the lumen between the outer and the underlying membrane. B: Membrane enlargement and wrinkling of the outer layer promotes PLY–membrane aggregated structures that induce strain by protein–protein interactions until the outer layer rips open (1) and layer-by-layer peeling (2), (red arrows) exposes the underlying layers for PLY attack. The diffusion of PLY monomers between multilamellar layers may also effect PLY binding to underlying layers and the association on the outer layer from below (3). The latter results in upside-down orientated pores. Thus, larger PLY–membrane aggregated structures were stabilized by back-to-back pore arrangements (4) interconnecting adjacent membrane undulations. C: Probable structures of multilamellar giant vesicles: stacked bilayers and two options of connected bilayers.

outer membrane to bind the layer underneath (green arrows). Thereby, the vesicle lumen becomes enriched with FITC-dextran (Fig. 5D, 03:52 min) too, demonstrating that active pores are present on both adjacent membranes. In summary, diverse effects of PLY on giant vesicles were observed, including protein–membrane aggregation (80.4%), layer-by-layer peeling (41.2%), vesicle collapse (25.5%) and vesicle enlargement (27.5%) (n = 51). Most of these membrane deformations were found together. At lower concentration of mCherry–PLY (160 nM, data not shown) these effects were delayed, as for instance the first peeling event requires incubation for about 3–4 min, which is much longer than observed with 320 nM mCherry–PLY (Fig. 2C and A).

Discussion

Binding of pneumolysin to giant vesicles resulted in several structural modifications such as membrane–protein aggregation, -enlargement, -deformation, -wrinkling, -peeling, and -interconnection.

In order to understand the mechanisms that may govern the membrane enlargements induced by PLY association, it should be acknowledged that PLY pores occupy a large areal fraction of solid-supported bilayers (SLB) shown by atomic force microscopy.[6] The dense arrangement of pores and pre-pores reported therein suggests that a large fraction of lipids must have been displaced from the SLB, which was also observed for other PFTs such as perforin,[49,50] suilysin, listerilysin-O and lysenin.[51] Such pore-displaced lipids would remain in the membrane or possibly re-intercalate into the vesicle bilayer rather than forming unfavorable micelles in aqueous solution. Moreover, some of those PFTs[52–54] also increased the surface pressure on Langmuir monolayers during insertion, which is indicative for membrane surface area enlargements.[55]

The possible interactions of PLY with the lipid membrane were summarized in a sketch (Fig. 6). These included initial homogeneous association to cholesterol, followed by the formation of open pores. Briefly, the pore-forming mechanisms[5,6] encompass the membrane association of monomeric PLY, oligomerization to arc[6] and ring structures and the assembly to early- and late pre-pores,[6] that eventually undergo transition to active pores (Fig. 6A). The inner diameter of pneumolysin pores is about 26 nm wide[6] and the approximate dimension of a PLY monomer in solution is 11.8 × 4.5 × 2.4 nm.[56] During PLY binding, membrane insertion and pore formation, the vesicle membrane surface area increased in order to maintain a constant spacing between membrane lipids and proteins. This effect appears to be different from membrane crowding, which induced membrane bending by lateral pressure generated by protein collision.[8,9] The probability that lipids, which were discriminated from the interior of pores, remain in the membrane may corroborate the formation of surplus membrane area on the outer layer of multilamellar giant vesicles. This expansion then promotes the development of an inter-membrane lumen (Fig. 6A, blue). Upon proceeding incubation

with further PLY, membrane wrinkles appear (Fig. 6B), that allow back-to-back pore assemblies due to protein–protein interactions. On multilamellar membranes, this might induce strain in the outer layer until it rips open (1) and peel off (2) to expose underlying layers for PLY incubation. Repetition of these processes results in layer-by-layer peeling of multilamellar giant vesicles. Furthermore, passive diffusion of monomers through pores into the inter-membrane lumen (3) also enables PLY to bind and form pores on the next underlying membrane layer as well as on the outer layer from the inner side, which eventually led to the formation of backward oriented pores. The capability of PLY pores and pre-pores to interconnect adjacent membranes intra-stabilizes large membrane wrinkles and also inter-connects different lamellae to support larger protein–membrane-aggregated structures (4). This results in the organization of mesh-like, interdigitating membrane lamellae and the formation of many membrane-enclosed lumina.

The formation of very large PLY-induced membrane wrinkles, which contain a lot of membrane bilayers (Fig. 4A, composite) indicates that lipid molecules may have been transferred from underlying, inner layers. This transfer might be supported by PLY-induced membrane fusion between lamellae after the formation of back-to-back pore arrangements or may suggest an MLV structure, where lamellae are connected to each other. In contrast to an onion-like organization of stacked layers, multilamellar vesicles may also have connected lamellae forming a stack of folded bilayers (Fig. 6C). The lipid transfer is indicated on a multilamellar vesicle that shows thinning of its membrane during the growth of surface-associated PLY–membrane wrinkles (Video SI 7,† arrow).

The diversity of PLY-induced alterations in the morphology of giant vesicles is likely to be affected by small alterations in the transition of pre-pores to active pores. Pre-pores bind and interconnect the membrane but only full pores might also displace pore-enclosed lipids and hence support intense membrane areal expansions.

Conclusions

In summary, we demonstrated that active pore-forming toxins such as pneumolysin, secreted by *Streptococcus pneumoniae* can deform and peel off multilamellar membranes. Membrane interactions include protein–membrane aggregation on the outer layer of multilamellar vesicles that causes bilayer expansion and wrinkling on the surface. Back-to-back pore interactions indicate that strain on the surface is induced, which led to membrane ripping and layer-by-layer peeling.

We also showed that the layer-by-layer peeling of multilamellar giant vesicles could be employed to determine the number of membrane layers. Moreover, the observed structural modifications of membranes are rather distinct from the toxins' well-known capability of forming pores and might inherit more versatile functionality to weaken the integrity of attacked membranes. Especially, the possibility that pores can

form on the outer layer of a multilamellar vesicle while PLY already diffuses through to bind and form pores on underlying membranes has further implications. Although having probed artificial high concentrations of lytic PLY, this points towards the possibility that the toxin secreted by *S. pneumoniae* exerts additional efficacy during a bacterial invasion on cells. Compartments that contain cholesterol,[33] such as endosomes, the Golgi or trafficking vesicles might become vulnerable when some initial pores on the plasma membrane would allow toxins to diffuse into the cytosol. This could play a role during toxin-induced cell lysis, when internal membrane repair mechanisms[17,18] were overwhelmed by high toxin loads.

Methods

Materials

1,2-Dioleoyl-*sn*-glycero-3-phosphocholine (DOPC), 1,2-dipalmi-toyl-*sn*-glycero-3-phosphocholine (DPPC), were received from Avanti Polar Lipids (Alabaster, AL, USA). Fluorescein isothio-cyanate (FITC)-dextran (70 kDa), dithiothreitol (DTT), Dulbecco's PBS, bovine serum albumin (BSA) and cholesterol were supplied by Sigma-Aldrich (Munich, Germany). [1,1′-Dioctadecyl-3,3,3′,3′-tetramethylindo-carbocyanine iodide] (DiI) was purchased from Ana Spec Inc. (Fremont, CA, USA). Poly(vinylalcohol) (PVA, 145 kDa) was obtained from Merck KGaA (Darmstadt, Germany) and BODIPY-PC from Thermo Fischer Scientific (Molecular Probes) (Thermo Scientific, Reinach, Switzerland). Human blood was from the Interregionale Blutspende SRK (Bern, Switzerland).

Protein expression and purification

Protein expression and purification followed an established protocol. Briefly, the constructs (pET28a-His6-mCherry-PLY, pET28a-His6-PLY,) containing the PLY sequence of S*treptococcus pneumoniae* strain D39[20] and pET28a-His6-LLO coding for listeriolysin-O, were transformed into BL21 (DE3) pLysS competent cells (Promega, Switzerland) and expression were induced by addition of 1 mM isopropyl β-D-1-thiogalacto-pyranoside (IPTG) (Sigma-Aldrich) at OD = 0.6 for 3 h at 37 °C. Cells were collected by centrifugation (3500*g*, 30 min, 4 °C) and lysed using lysozyme and DNAse I (Sigma-Aldrich) fol-lowed by 10 × 20 s sonication steps with 15 s breaks (on ice) (BANDELIN SONOPULS UW 2070, BANDELIN Electronic GmbH & Co. KG, Berlin, Germany). After ultracentrifugation (70 000*g*, 1 h, 4 °C) the protein was purified with Protino® Ni-NTA 1 ml columns (MACHEREY-NAGEL, Oensingen, Switzerland) using an ÄKTAprime plus (GE Healthcare, Little Chalfont, UK). After dialysis in PBS (MWCO 12 kDa, overnight, 4 °C, Sigma–Aldrich) bacterial endotoxin was removed by Pierce® High-Capacity Endotoxin Removal Spin Columns (Thermo Scientific, Rockford, IL, USA). SDS-PAGE and western blotting (1F11 mouse anti PLY IgG, Santa Cruz Biotechnology, Dallas, TX, USA), WesternBright™ ECL detection kit, Advansta Inc., CA, USA confirmed protein purity (≥95%). PLY constructs were activated in the presence of 1 mM DTT and used immedi-

ately. Similar membrane affinity was probed by hemolytic activity.[22] Y221G-aerolysin-EGFP was purified as described.[57] The pET28-His6-EGFP-Lys(169-297) (EGFP-NT-LYS) construct was purchased from RIKEN (Wako, Saitama, Japan) and EGFP-NT-LYS was purified employing a modified protocol as described.[46] Briefly, the construct was transformed into BL21 (DE3) pLysS competent cells (Promega, Switzerland); growth was followed until OD = 0.6 at 37 °C; expression was induced by 0.2 mM IPTG at 25 °C for 6 h. Purification was performed as described for PLY, including endotoxin removal.

Pre-sequestration hemolytic assay

An established protocol was modified as follows.[22] Briefly, liposomes (≈90 nM–188 µM) were pre-incubated with 16 nM mCherry–PLY in the presence of 2.5 mM DTT at RT. After 15 min pre-incubation time, the addition (1 : 1 v/v) of 2% hRBCs initiated hemolysis. The mixture containing 1% hRBCs and 8 nM PLY (sufficient for 100% lysis) was then incubated for 30 min at 37 °C. Centrifugation and measurement of hemolysis was performed as described[20] and normalized hemolytic data were analyzed by the nonlinear regression of (symmetrical) sigmoidal dose–response curves with variable Hill slope using GraphPad Prism 7 (ESI; Table SI 1†).

Preparation of liposomes and giant vesicles

Lipid stocks were handled in chloroform/methanol (1 : 1 v/v) and mixed in a molar ratio. Liposomes were prepared by extru-sion using a 200 nm polycarbonate membrane employing a LiposoFast-Basic extrusion system (Avestin Europe GmbH, Mannheim, Germany) as reported earlier.[58] Giant vesicles were prepared using a modified protocol.[22,59,60] Briefly, a thin film of poly(vinyl alcohol) (PVA) is prepared by drying 30–50 µl of a 5% (w/v) PVA solution in ultrapure water at 80 °C on a glass slide (1 cm²). The film is dried for 5 min at 40–50 °C and the lipid mixture was deposited until the solvent evaporated. The film was then dried (60 min, RT, vacuum) and vesicles were swollen in PBS pH 7.4 buffer at 50–60 °C for 1 h. Multilamellar vesicles were preferentially chosen for this study.

Dynamic light scattering

Liposomes (DOPC/Chol, 50 : 50, 0.6 mM) were prepared by extrusion, 31× through a 200 nm polycarbonate membrane (Avanti Polar Lipids) in PBS and diluted to 0.25 mM. PLY was activated in the presence of DTT and incubated with 0.25 mM DOPC/Chol (50 : 50) liposomes for 5 min at RT. Dynamic light scattering was measured at 25 °C (Zetasizer Nano ZSP, Malvern Panalytical Ltd, Malvern, UK) and data were analyzed (Zetasizer Software 7.11) before a mean of 5 experiments is used to calculate a Gaussian distribution (R^2 = 0.98–0.99). Buffers have been filtrated (pore Ø = 0.2 µm) and degassed. Errors = S.D.

Microfluidic experiments using giant vesicles

An established microfluidic chip design[29] was modified to increase the probability of vesicle immobilization as described.[22] The device is actuated using nitrogen at a

pressure of 200 kPa employing a custom-made pressure valve control instrument.[22] Chip fabrication followed an established protocol as described.[22,29,61] Compounds were injected using a syringe-pump system (NanoJet syringe pump, Chemyx, Stafford, TX, USA) and Teflon tubes. Ultrapure water was added to the fluid layer and pressure control openings before operation by centrifugation (700g, 5 min, RT) to circumvent air pockets.[29,61] The device was mounted onto the microscope stage holder (equilibrated to T = 28 °C) and channels were coated by 4% (w/v) BSA in PBS at a flow of 10 μl min^{-1} for 10 minutes. Giant vesicles were then trapped from PBS solution at 2 μl min^{-1} and experiments were performed at a flow rate of 0.125 μl min^{-1} per chamber. This did not apply any observable shear stress on the liposomes[30] and did not affect large PLY–membrane aggregated structures.

Microscopy

The microfluidic devices were mounted on the stage of a microscope (Zeiss LSM 880), equipped with a temperature-controlled incubation chamber and a Plan APO 63×/1.4 Oil DIC M27 objective (Carl Zeiss Microscopy GmbH, Jena, Germany). For the excitation of mCherry or DiI, a 561 nm diode pumped solid state (DPSS) laser (BP 578 nm–696 nm) was employed. For FITC or EGFP, the 488 nm line of the argon laser (BP 493 nm–556 nm) and the beamsplitter MBS 488/561 were used. Image processing included the Zeiss ZEN 2 software (Carl Zeiss Microscopy GmbH 1997–2014) and Fiji. Fluorescence images have been contrast enhanced to optimize presentation (equatorial section, if not otherwise stated). Experiments were performed at T = 28 ± 1 °C.

Cryo-transmission electron microscopy

Liposomes have been prepared in PBS (2 mM) by extrusion using a 200 nm polycarbonate membrane employing a LiposoFast-Basic extrusion system (Avestin Europe GmbH, Mannheim, Germany) or by sonication, 3 pulses at 30 s (BANDELIN Sonopuls UW 2070, BANDELIN Electronic GmbH & Co. KG, Berlin, Germany) and were mixed with 1 μM PLY in the presence of 2 mM DTT in PBS and incubated 10 min at 37 °C. Subsequently, 3 μl of the mixtures were applied to a 2/1 quantifoil grid (Quantifoil Microtools GmbH) after 15″15 mA glow discharging. The grids were then plunge-frozen using a Vitrobot (FEI – Thermo Fisher) employing 2 to 5 s blotting time, 100% humidity, 2 s wait step and 2 s drain times, respectively. The cryo grids were imaged on an F20 microscope (FEI – Thermo Fischer) equipped with a Falcon III direct detector. Images were acquired in the nanoprobe mode with total doses ranging from 30 e$^-$ Å^{-1} to 90 e$^-$ Å^{-1}.

Author contributions

P. D., I. I., S. B. and E. B. B. performed and analyzed *in vitro* experiments. P. D., B. Z., E. B. B., P. S. D. and A. D. designed the study and wrote the paper. P. D. and A. D. coordinated the study. All authors analyzed and discussed the results and commented on the manuscript.

Conflicts of interest

There are no conflicts to declare.

Acknowledgements

References

1 T. M. Weaver, J. M. Hocking, L. J. Bailey, G. T. Wawrzyn, D. R. Howard, L. A. Sikkink, *et al.*, Structural and Functional Studies of Truncated Hemolysin A from *Proteus mirabilis*, *J. Biol. Chem.*, 2009, **284**(33), 22297–22309.

2 B. König, A. Ludwig, W. Goebel and W. König, Pore formation by the *Escherichia coli* alpha-hemolysin: role for mediator release from human inflammatory cells, *Infect. Immun.*, 1994, **62**(10), 4611–4617.

3 S. A. Glazier, D. J. Vanderah, A. L. Plant, H. Bayley, G. Valincius and J. J. Kasianowicz, Reconstitution of the pore-forming toxin α-Hemolysin in phospholipid/18-octadecyl-1-thiahexa(ethylene oxide) and phospholipid/n-octadecanethiol supported bilayer membranes, *Langmuir*, 2000, **16**(26), 10428–10435.

4 R. Thompson James, B. Cronin, H. Bayley and I. Wallace Mark, Rapid Assembly of a Multimeric Membrane Protein Pore, *Biophys. J.*, 2011, **101**(11), 2679–2683.

5 S. J. Tilley, E. V. Orlova, R. J. C. Gilbert, P. W. Andrew and H. R. Saibil, Structural Basis of Pore Formation by the Bacterial Toxin Pneumolysin, *Cell*, 2005, **121**(2), 247–256.

6 K. van Pee, E. Mulvihill, D. J. Müller and Ö. Yildiz, Unraveling the Pore-Forming Steps of Pneumolysin from Streptococcus pneumoniae, *Nano Lett.*, 2016, **16**(12), 7915–7924.

7 S. D. Taylor, M. E. Sanders, N. A. Tullos, S. J. Stray, E. W. Norcross, L. S. McDaniel, *et al.*, The Cholesterol-Dependent Cytolysin Pneumolysin from *Streptococcus pneumoniae* Binds to Lipid Raft Microdomains in Human Corneal Epithelial Cells, *PLoS One*, 2013, **8**(4), e61300.

8 J. C. Stachowiak, E. M. Schmid, C. J. Ryan, H. S. Ann, D. Y. Sasaki, M. B. Sherman, *et al.*, Membrane bending by

protein–protein crowding, *Nat. Cell Biol.*, 2012, **14**(9), 944–949.

9   H.-X. Zhou, Crowding effects of membrane proteins, *J. Phys. Chem. B*, 2009, **113**(23), 7995–8005.

10 T. L. Boye, K. Maeda, W. Pezeshkian, S. L. Sønder, S. C. Haeger, V. Gerke, *et al.*, Annexin A4 and A6 induce membrane curvature and constriction during cell membrane repair, *Nat. Commun.*, 2017, **8**(1), 1623.

11 P. A. Beales, C. L. Bergstrom, N. Geerts, J. T. Groves and T. K. Vanderlick, Single Vesicle Observations of the Cardiolipin−Cytochrome c Interaction: Induction of Membrane Morphology Changes, *Langmuir*, 2011, **27**(10), 6107–6115.

12 J. A. Jackman, H. Z. Goh, V. P. Zhdanov, W. Knoll and N.-J. Cho, Deciphering How Pore Formation Causes Strain-Induced Membrane Lysis of Lipid Vesicles, *J. Am. Chem. Soc.*, 2016, **138**(4), 1406–1413.

13 J. E. Marshall, B. H. A. Faraj, A. R. Gingras, R. Lonnen, M. A. Sheikh, M. El-Mezgueldi, *et al.*, The Crystal Structure of Pneumolysin at 2.0 Å Resolution Reveals the Molecular Packing of the Pre-pore Complex, *Sci. Rep.*, 2015, **5**, 13293.

14 K. van Pee, A. Neuhaus, E. D'Imprima, D. J. Mills, W. Kühlbrandt and Ö. Yildiz, CryoEM structures of membrane pore and prepore complex reveal cytolytic mechanism of pneumolysin, *eLife*, 2017, **6**, e23644.

15 I. Iacovache, S. De Carlo, N. Cirauqui, M. Dal Peraro, F. G. van der Goot and B. Zuber, Cryo-EM structure of aerolysin variants reveals a novel protein fold and the pore-formation process, *Nat. Commun.*, 2016, **7**, 12062.

16 B. D. Henry, D. R. Neill, K. A. Becker, S. Gore, L. Bricio-Moreno, R. Ziobro, *et al.*, Engineered liposomes sequester bacterial exotoxins and protect from severe invasive infections in mice, *Nat. Biotechnol.*, 2015, **33**(1), 81–88.

17 A. Draeger, R. Schoenauer, A. P. Atanassoff, H. Wolfmeier and E. B. Babiychuk, Dealing with damage: Plasma membrane repair mechanisms, *Biochimie*, 2014, **107**(Part A), 66–72.

18 E. B. Babiychuk and A. Draeger, Defying death: Cellular survival strategies following plasmalemmal injury by bacterial toxins, *Semin. Cell Dev. Biol.*, 2015, **45**, 39–47.

19 H. Wolfmeier, R. Schoenauer, A. P. Atanassoff, D. R. Neill, A. Kadioglu, A. Draeger, *et al.*, Ca2+-dependent repair of pneumolysin pores: A new paradigm for host cellular defense against bacterial pore-forming toxins, *Biochim. Biophys. Acta, Mol. Cell Res.*, 2015, **1853**(9), 2045–2054.

20 H. Wolfmeier, J. Radecke, R. Schoenauer, R. Koeffel, V. S. Babiychuk, P. Drücker, *et al.*, Active release of pneumolysin prepores and pores by mammalian cells undergoing a *Streptococcus pneumoniae*, *Biochim. Biophys. Acta, Gen. Subj.*, 2016, **1860**(11, Part A), 2498–2509.

21 E. B. Babiychuk, K. Monastyrskaya, S. Potez and A. Draeger, Blebbing confers resistance against cell lysis, *Cell Death Differ.*, 2011, **18**(1), 80–89.

22 P. Drücker, S. Bachler, H. Wolfmeier, R. Schoenauer, R. Köffel, V. S. Babiychuk, *et al.*, Pneumolysin-damaged cells benefit from non-homogeneous toxin binding to cholesterol-rich membrane domains, *Biochim. Biophys. Acta, Mol. Cell Biol. Lipids*, 2018, **1863**(8), 795–805.

23 S. F. Fenz and K. Sengupta, Giant vesicles as cell models, *Integr. Biol.*, 2012, **4**(9), 982–995.

24 O. Jalmar, A. J. García-Sáez, L. Berland, F. Gonzalvez and P. X. Petit, Giant unilamellar vesicles (GUVs) as a new tool for analysis of caspase-8/Bid-FL complex binding to cardiolipin and its functional activity, *Cell Death Dis.*, 2010, **1**(12), e103.

25 M. Chiba, M. Miyazaki and S. Ishiwata, Quantitative Analysis of the Lamellarity of Giant Liposomes Prepared by the Inverted Emulsion Method, *Biophys. J.*, 2014, **107**(2), 346–354.

26 P. Kuhn, K. Eyer and P. S. Dittrich, A microfluidic device for the delivery of enzymes into cells by liposome fusion, *Eng. Life Sci.*, 2018, **18**(2), 149–156.

27 M. Pillong, J. A. Hiss, P. Schneider, Y.-C. Lin, G. Posselt, B. Pfeiffer, *et al.*, Rational Design of Membrane-Pore-Forming Peptides, *Small*, 2017, **13**(40), 1701316.

28 K. Eyer, F. Paech, F. Schuler, P. Kuhn, R. Kissner, S. Belli, *et al.*, A liposomal fluorescence assay to study permeation kinetics of drug-like weak bases across the lipid bilayer, *J. Controlled Release*, 2014, **173**, 102–109.

29 T. Robinson, P. Kuhn, K. Eyer and P. S. Dittrich, Microfluidic trapping of giant unilamellar vesicles to study transport through a membrane pore, *Biomicrofluidics*, 2013, **7**(4), 044105.

30 F. Sturzenegger, T. Robinson, D. Hess and P. S. Dittrich, Membranes under shear stress: visualization of non-equilibrium domain patterns and domain fusion in a microfluidic device, *Soft Matter*, 2016, **12**(23), 5072–5076.

31 B. Sebastian, T. Favero and P. S. Dittrich, The Effects of Shear Force Transmission Across Vesicle Membranes, *J. Phys. Chem. Lett.*, 2017, **8**(24), 6128–6134.

32 K. Akashi, H. Miyata, H. Itoh and K. Kinosita, Preparation of giant liposomes in physiological conditions and their characterization under an optical microscope, *Biophys. J.*, 1996, **71**(6), 3242–3250.

33 G. van Meer, D. R. Voelker and G. W. Feigenson, Membrane lipids: where they are and how they behave, *Nat. Rev. Mol. Cell Biol.*, 2008, **9**(2), 112–124.

34 A. A. Spector and M. A. Yorek, Membrane lipid composition and cellular function, *J. Lipid Res.*, 1985, **26**(9), 1015–1035.

35 T. Bhatia, P. Husen, J. Brewer, L. A. Bagatolli, P. L. Hansen, J. H. Ipsen, *et al.*, Preparing giant unilamellar vesicles (GUVs) of complex lipid mixtures on demand: Mixing small unilamellar vesicles of compositionally heterogeneous mixtures, *Biochim. Biophys. Acta, Biomembr.*, 2015, **1848**(12), 3175–3180.

36 P. Walde, K. Cosentino, H. Engel and P. Stano, Giant Vesicles: Preparations and Applications, *ChemBioChem*, 2010, **11**(7), 848–865.

37 A. Fischer, T. Oberholzer and P. L. Luisi, Giant vesicles as models to study the interactions between membranes and proteins, *Biochim. Biophys. Acta, Biomembr.*, 2000, **1467**(1), 177–188.

38 N. F. Morales-Penningston, J. Wu, E. R. Farkas, S. L. Goh, T. M. Konyakhina, J. Y. Zheng, *et al.*, GUV preparation and imaging: Minimizing artifacts, *Biochim. Biophys. Acta*, 2010, **1798**(7), 1324–1332.

39 T. Wollert, C. Wunder, J. Lippincott-Schwartz and J. H. Hurley, Membrane Scission by the ESCRT-III Complex, *Nature*, 2009, **458**(7235), 172–177.

40 M. Bokori-Brown, P. G. Petrov, M. A. Khafaji, M. K. Mughal, C. E. Naylor, A. C. Shore, *et al.*, Red Blood Cell Susceptibility to Pneumolysin: Correlation with Membrane Biochemical and Physical Properties, *J. Biol. Chem.*, 2016, **291**(19), 10210–10227.

41 J. Huang, Model Membrane Thermodynamics and Lateral Distribution of Cholesterol: From Experimental Data To Monte Carlo Simulation, *Methods Enzymol.*, 2009, **455**, 329–364.

42 J. Huang and G. W. Feigenson, A Microscopic Interaction Model of Maximum Solubility of Cholesterol in Lipid Bilayers, *Biophys. J.*, 1999, **76**(4), 2142–2157.

43 C. I. McPhee, G. Zoriniants, W. Langbein and P. Borri, Measuring the Lamellarity of Giant Lipid Vesicles with Differential Interference Contrast Microscopy, *Biophys. J.*, 2013, **105**(6), 1414–1420.

44 L.-A. S. Kirkham, A. R. Kerr, G. R. Douce, G. K. Paterson, D. A. Dilts, D.-F. Liu, *et al.*, Construction and Immunological Characterization of a Novel Nontoxic Protective Pneumolysin Mutant for Use in Future Pneumococcal Vaccines, *Infect. Immun.*, 2006, **74**(1), 586–593.

45 H. Shogomori and T. Kobayashi, Lysenin: A sphingomyelin specific pore-forming toxin, *Biochim. Biophys. Acta, Gen. Subj.*, 2008, **1780**(3), 612–618.

46 A. Makino, M. Abe, M. Murate, T. Inaba, N. Yilmaz, F. Hullin-Matsuda, *et al.*, Visualization of the heterogeneous membrane distribution of sphingomyelin associated with cytokinesis, cell polarity, and sphingolipidosis, *FASEB J.*, 2015, **29**(2), 477–493.

47 J. Drazenovic, H. Wang, K. Roth, J. Zhang, S. Ahmed, Y. Chen, *et al.*, Effect of lamellarity and size on calorimetric phase transitions in single component phosphatidyl-choline vesicles, *Biochim. Biophys. Acta, Biomembr.*, 2015, **1848**(2), 532–543.

48 U. Kauscher, M. C. A. Stuart, P. Drücker, H.-J. Galla and B. J. Ravoo, Incorporation of Amphiphilic Cyclodextrins into Liposomes as Artificial Receptor Units, *Langmuir*, 2013, **29**(24), 7377–7383.

49 C. Leung, A. W. Hodel, A. J. Brennan, N. Lukoyanova, S. Tran, C. M. House, *et al.*, Real-time visualization of perforin nanopore assembly, *Nat. Nanotechnol.*, 2017, **12**(5), 467–473.

50 A. W. Hodel, C. Leung, N. V. Dudkina, H. R. Saibil and B. W. Hoogenboom, Atomic force microscopy of membrane pore formation by cholesterol dependent cytolysins, *Curr. Opin. Struct. Biol.*, 2016, **39**, 8–15.

51 N. Yilmaz and T. Kobayashi, Assemblies of pore-forming toxins visualized by atomic force microscopy, *Biochim. Biophys. Acta, Biomembr.*, 2016, **1858**(3), 500–511.

52 M. Hereć, M. Gagoś, M. Kulma, K. Kwiatkowska, A. Sobota and W. I. Gruszecki, Secondary structure and orientation of the pore-forming toxin lysenin in a sphingomyelin-containing membrane, *Biochim. Biophys. Acta, Biomembr.*, 2008, **1778**(4), 872–879.

53 A. Bavdek, N. O. Gekara, D. Priselac, I. Gutiérrez Aguirre, A. Darji, T. Chakraborty, *et al.*, Sterol and pH Interdependence in the Binding, Oligomerization, and Pore Formation of Listeriolysin O, *Biochemistry*, 2007, **46**(14), 4425–4437.

54 A. Barlič, I. Gutiérrez-Aguirre, J. M. M. Caaveiro, A. Cruz, M.-B. Ruiz-Argüello, J. Pérez-Gil, *et al.*, Lipid Phase Coexistence Favors Membrane Insertion of Equinatoxin-II, a Pore-forming Toxin from Actinia equina, *J. Biol. Chem.*, 2004, **279**(33), 34209–34216.

55 R. K. Harishchandra, M. Saleem and H.-J. Galla, Nanoparticle interaction with model lung surfactant monolayers, *J. R. Soc., Interface*, 2010, **7**(Suppl 1), S15–S26.

56 A. S. Solovyova, M. Nöllmann, T. J. Mitchell and O. Byron, The Solution Structure and Oligomerization Behavior of Two Bacterial Toxins: Pneumolysin and Perfringolysin O, *Biophys. J.*, 2004, **87**(1), 540–552.

57 I. Iacovache, M. T. Degiacomi, L. Pernot, S. Ho, M. Schiltz, M. Dal Peraro, *et al.*, Dual Chaperone Role of the C-Terminal Propeptide in Folding and Oligomerization of the Pore-Forming Toxin Aerolysin, *PLoS Pathog.*, 2011, **7**(7), e1002135.

58 P. Drücker, D. Grill, V. Gerke and H.-J. Galla, Formation and Characterization of Supported Lipid Bilayers Containing Phosphatidylinositol-4,5-bisphosphate and Cholesterol as Functional Surfaces, *Langmuir*, 2014, **30**(49), 14877–14886.

59 A. Weinberger, F.-C. Tsai, H. Koenderink Gijsje, F. Schmidt Thais, R. Itri, W. Meier, *et al.*, Gel-Assisted Formation of Giant Unilamellar Vesicles, *Biophys. J.*, 2013, **105**(1), 154–164.

60 P. Drücker, M. Pejic, H.-J. Galla and V. Gerke, Lipid segregation and membrane budding induced by the peripheral membrane binding protein Annexin A2, *J. Biol. Chem.*, 2013, **288**(34), 24764–24776.

61 K. Eyer, P. Kuhn, C. Hanke and P. S. Dittrich, A microchamber array for single cell isolation and analysis of intracellular biomolecules, *Lab Chip*, 2012, **12**(4), 765–772.